HHS Public Access

Author manuscript

Biochemistry. Author manuscript; available in PMC 2019 June 05.

Published in final edited form as:

Biochemistry. 2018 June 05; 57(22): 3146–3154. doi:10.1021/acs.biochem.8b00142.

Dynamic characteristics of GMP reductase complexes revealed by high resolution ^{31}P field cycling NMR relaxometry

Masha M. Rosenberg[‡], **Alfred G. Redfield**[§], **Mary F. Roberts**[¶,*], and **Lizbeth Hedstrom**[‡,£,*]

[‡] Department of Biology, Brandeis University, MS009, 415 South St., Waltham MA 02453-9110 USA

[§] Department of Biochemistry, Brandeis University, MS009, 415 South Street, Waltham, MA 02453-9110 USA

[¶] Department of Chemistry, Boston College, 140 Commonwealth Avenue, Chestnut Hill, MA 02467-9110 USA

[£] Department of Chemistry, Brandeis University, 415 South Street, Waltham, MA 02453-3808 USA.

Abstract

The ability of enzymes to modulate the dynamics of bound substrates and cofactors is a critical feature of catalysis, but the role of dynamics has largely been approached from the perspective of the protein. Here we use an underappreciated NMR technique, subtesla high resolution field cycling ^{31}P NMR relaxometry, to interrogate the dynamics of enzyme bound substrates and cofactors in guanosine-5'-monophosphate reductase (GMPR). These experiments reveal distinct binding modes and dynamic profiles associated with the ^{31}P nuclei in the Michaelis complexes for the deamination and hydride transfer steps of the catalytic cycle. Importantly, the substrate is constrained and the cofactor is more dynamic in the deamination complex E•GMP•NADP$^+$, while the substrate is more dynamic and the cofactor is constrained in the hydride transfer complex E•IMP•NADP$^+$. The presence of D_2O perturbed the relaxation of the ^{31}P nuclei in E•IMP•NADP$^+$, but not in E•GMP•NADP$^+$, providing further evidence of distinct binding modes, with different dynamic properties. dIMP and dGMP are poor substrates, and the dynamics of the cofactor complexes of dGMP/dIMP are disregulated relative to GMP/IMP. The substrate 2'-OH interacts with Asp219, and mutation of Asp219 to Ala decreases the value of V_{max} by a factor of 30. Counterintuitively, loss of Asp219 makes both substrates and cofactors less dynamic. These observations suggest that the interactions between the substrate 2'-OH and Asp219 coordinate the dynamic properties of the Michaelis complexes, and these dynamics are important for progression through the catalytic cycle.

[*]To whom correspondence should be addressed: Lizbeth Hedstrom, Department of Biology, Brandeis University, MS009, 415 South Street, Waltham, MA 02453-9110 USA. Tel: 781-736-2333; Fax: 781-736-2349; hedstrom@brandeis.edu; Mary Roberts, Department of Chemistry, Boston College, 140 Commonwealth Avenue, Chestnut Hill, MA 02467-9110. Tel: 617-552-3616; mary.roberts@bc.edu.

Author contributions: MMR, AR and MFR designed the NMR experiments; AGR built the field cycling apparatus. MMR conducted the experiments, MMR and MFR analyzed the NMR data. LH conceived the idea for the project. MMR, MFR and LH wrote the paper.

Supporting Information. Extrapolated ^{31}P-^{1}H distances, pre-steady state progress curves.

Conflict of interest: The authors declare that they have no conflicts of interest with the contents of this article.

TOC Graphic

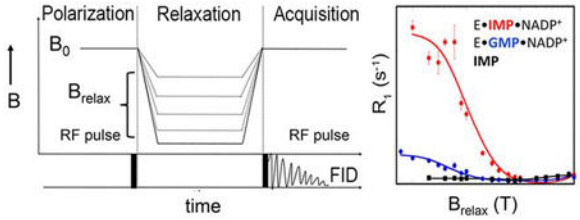

Keywords

oxidoreductases; enzyme catalysis; NMR spectroscopy; cofactor dynamics

INTRODUCTION

Much of the remarkable power and specificity of enzyme catalysis derives from interactions with portions of substrates that are removed from the site of chemical transformation. This phenomenon distinguishes on-enzyme reactions from those in solution. Several general mechanisms can be envisioned to explain how the binding energy of remote interactions is harnessed to promote catalysis. (1) Distal portions of the protein can exert their effects on the ground state by serving as anchors tethering the substrate to the active site, as exemplified by ketosteroid isomerase [1]. Such interactions can enforce productive binding modes that properly position the substrate relative to the catalytic machinery. (2) Distal interactions can induce conformational changes that organize the active site, stabilizing the structure of mobile loops and positioning key catalytic residues. Such conformational changes often create “cages” that envelope the substrate and exclude solvent [2]. (3) Distal portions of the substrate can stabilize the transition state if their interactions with the protein are optimized in the transition state, as observed in tyrosyl-tRNA synthetase [3]. (4) Distal substrate moieties may also contribute to the electrostatic environment of the active site. (5) Lastly, it is not difficult to imagine that distal portions of the substrate could potentially couple motions across the active site.

The ability of enzymes to modulate the dynamics of bound substrates and cofactors is a critical feature of catalysis. Nonetheless, the role of dynamics in enzyme catalysis has largely been approached from the perspective of the protein. Here we use an underappreciated NMR technique, subtesla high resolution field cycling ^{31}P NMR relaxometry [4, 5678, 910], to interrogate the dynamics of enzyme bound substrates and cofactors in guanosine-5’-monophosphate reductase (GMPR). This enzyme presents an excellent system to investigate the dynamics of enzyme-bound ligands because the cofactor has different conformations during the two steps of the catalytic cycle.

GMPR is a triose phosphate isomerase (TIM) barrel protein, the most common enzyme fold, and contains the standard phosphate “gripper” loop found throughout this superfamily [11, 12]. The enzyme is a square planar homotetramer with four active sites. The GMP/IMP and nicotinamide binding sites lie within one monomer while the binding site for the adenosine portion of the cofactor is in the adjacent subunit. This enzyme catalyzes two different

chemical transformations (Figure 1A) [13]. The first step is a deamination reaction, where the catalytic residue Cys186 attacks C2 of GMP to create a covalent thioimidate intermediate (E-XMP*) and ammonia (Figure 1A). The cofactor is present for the deamination reaction, but the nicotinamide must be positioned away from GMP to allow deamination to proceed. Then the nicotinamide moves adjacent to C2 of E-XMP* to allow hydride transfer and production of IMP. The x-ray crystal structure of the inactive E•IMP•NADPH complex captures the cofactor in two conformations, an "OUT" conformation believed to be used in the deamination reaction and an "IN" conformation that appears competent for hydride transfer (Figure 1B) [13]. However, the relevance of these structures to catalysis remains to be established.

Our previously reported field cycling experiments interrogated the $NADP^+$ complexes of both GMP and IMP [4]. These complexes undergo partial reactions that resemble different steps in the full catalytic cycle (Figure 1C) [13]: (1) E•GMP•$NADP^+$ undergoes a partial deamination reaction to form E-XMP*•NH_3•$NADP^+$. This partial reaction requires that the cofactor nicotinamide is positioned away from GMP, as observed in the OUT structure. (2) E•IMP•$NADP^+$ undergoes a partial hydride transfer reaction to form E-XMP*•NADPH in the absence of ammonia. This reaction requires the nicotinamide to be adjacent to IMP, as observed in the IN structure. The field cycling experiments revealed that the monophosphates of IMP and GMP have distinct binding modes in these cofactor complexes. This finding was not anticipated by the x-ray crystal structures, where the IMP and GMP monophosphate binding sites are virtually identical [1314]. Contrary to expectations, we could not detect differences in the cofactor binding mode, although different dynamic processes are associated with the cofactor in each complex [4]. Most intriguingly, the dynamics of the substrate and cofactor are coordinately regulated. In the deamination complex, GMP is relatively constrained while the cofactor is dynamic. In contrast, IMP is dynamic and the cofactor is constrained in the hydride transfer complex. Here we show that the substitution of either the substrate 2'-OH or Asp219 compromises catalysis, and the associated binding modes and dynamic profiles of the ^{31}P nuclei are no longer congruous with the requisite chemical transformations.

MATERIALS/EXPERIMENTAL DETAILS

Materials –

$NADP^+$ was obtained from Roche Diagnostics. IMP was purchased from MP Biomedicals. GMP, dGMP, dIMP and NADPH were purchased from Sigma. D_2O (99.9%) and deuterated Tris-d_{11} (98%) were obtained from Cambridge Isotopes.

Overexpression and purification of WT and D219A GMPR –

Expression and purification of recombinant *E. coli* GMPR was carried out as described previously [4]. In brief, His-tagged protein was purified using Ni-NTA agarose resin (Molecular Cloning Laboratories, Inc.). Enzyme was dialyzed against 75 mM Tris-HCl, pH 7.8, 100 mM KCl, 1 mM DTT, 0.5 mM EDTA, 5% glycerol and stored at −20 °C. The protein purity was verified by SDS-gel electrophoresis. The protein concentration was

determined by A_{280} using the extinction coefficient calculated with ProtParam [15]. Protein was concentrated using Amicon Ultra centrifugal 10K filters for NMR samples.

High-resolution ^{31}P field-cycling NMR measurements –

Samples contained 400 μM GMPR and 1.6 mM ligands in 75 mM Tris-HCl, pH 7.8, with 100 mM KCl, 1 mM DTT and 0.5 mM EDTA in 24% D_2O. For D_2O experiments, deuterated Tris-d_{11} and 100% of D_2O were used. The ^{31}P field-cycling spin-lattice relaxation rate (R_1) measurements were taken at 25 °C on a Varian INOVA 500 spectrometer using a standard 10 mm Varian probe in a device that was built to move the sample from the conventional sample probe location at 11.7 T, to a higher position where the magnetic field can be as low as 0.04 T [5]. A permanent magnet was mounted at the top of the dewar to program fields between 0.003 and 0.04 T. Relaxation experiments were typically 3 to 6 hours long at a given field strength (longer times required at the lowest magnetic fields), each with 5 to 7 programmed delay times, starting at low field and continuing to progressively higher field. Data were analyzed with an exponential function to extract the spin-lattice relaxation rate $R_1 = 1/T_1$.

^{31}P field-cycling NMR data analysis –

Spectra were plotted and intensities were measured by Vnmr 6.1B software. The dependence of R_1 on magnetic field allows the extraction of an effective correlation time (τ) for the ligand bound to GMPR and a dipolar relaxation rate extrapolated for zero field (R_0), as described by the following equation:

$$R_1 = [R_0/2\tau]\{0.1J(\tau, \omega_H-\omega_P) + 0.3J(\tau, \omega_P) + 0.6J(\tau, \omega_H+\omega_P)\}+\text{CSA} \quad [1]$$

where $\text{CSA} = C_L\omega_P^2 J(\omega_P) + C_H \omega_P^2 H^2$. Here $J(\tau,\omega)$ is the spectral density function and equal to $2\tau/(1+\omega_P^2\tau^2)$, C_L and C_H are low-frequency and high-frequency contributions of the CSA interaction to relaxation, respectively, and ω_H and ω_P are the proton and ^{31}P gyromagnetic ratios multiplied by magnetic field, H (in T). The contribution $C_L\omega_P^2 J(\omega_P)$ was introduced to account for relaxation occurring in the region from 0.5 to 4 T that could otherwise not be accounted for by dipolar and the CSA detected at high fields [16]. As such it is an empirical ‘correction’. In this work, we ignore CSA except to improve fits of the data. An averaged distance from the nearest protons to the ^{31}P is proportional to the sixth root of τ/R_0:

$$r_{eff}^6=(\mu_0/4\pi)^2(h/2\pi)^2\gamma_P^2\gamma_H^2\tau/R_0 \quad [2]$$

where h is Planck`s constant and μ_0 is the permeability of free space, and γ_P and γ_H are the gyromagnetic ratios for ^{31}P and ^{1}H, respectively. We define r_{eff}, as the on-enzyme distance between the ^{31}P and nearby protons that are responsible for the dipolar relaxation. It is not normalized to a specific number of protons, since that is not known. However, it does provide a way to compare different substrates and the effect of removing exchangeable protons from the system.

Enzyme Kinetics –

Steady state GMPR analyses were conducted at 25 °C in 75 mM Tris, pH 7.8, 100 mM KCl, 1 mM DTT and 0.5 mM EDTA. Enzyme activity was monitored spectrophotometrically at 340 nm. Initial velocity data were fit to the Michaelis-Menten equation (eq. [3]) where v is the initial velocity, V_m is the maximal velocity, K_m is the Michaelis constant and [S] is the substrate concentration.

$$v = V_m[S]/(K_m + [S]) \quad [3]$$

Pre-steady state kinetics were performed on a stopped-flow spectrophotometer (Applied Photophysics SX.17MV). The reaction was monitored by absorbance at 340 nm at 25 °C. GMPR was mixed with an equal volume of saturating substrates (final concentrations = 10 μM, 500 μM and 500 μM for wildtype GMPR, IMP and $NADP^+$, respectively; 10 μM, 500 μM and 500 μM for wildtype GMPR, dIMP and $NADP^+$, respectively; 30 μM, 10 mM and 3 mM for D219A mutant, IMP and $NADP^+$, respectively). The data were fit to single exponential (Equation 4) for the GMPR+IMP+$NADP^+$ and GMPR+dIMP+$NADP^+$ reactions.

$$A_t = A_0(1 - \exp(-k_{obs} \bullet t)) \quad [4]$$

Here A_t is the absorbance at 340 nm at time t, A_0 is the maximum absorbance, and k_{obs} is the observed rate constant of the reaction. Data from the D219A+IMP+$NADP^+$ reaction were fit to a single exponential plus steady state equation:

$$A_t = A_0(1 - \exp(-k_{obs} \bullet t)) + B\,t + C \quad [5]$$

where A_0 is the maximum absorbance at 340 nm and k_{obs} is an observed rate constant of the exponential part, B is the steady state rate constant, and C is the basal absorbance.

RESULTS AND DISCUSSION

Overview of high resolution field cycling.

For a small molecule in solution, the ^{31}P spin-lattice relaxation rate (R_1) is dominated by chemical shift anisotropy (CSA) in high magnetic fields. In low magnetic fields, both the CSA and the dipolar contribution to relaxation of the small molecule phosphorus are inefficient, so R_1 is very small. However, if the small molecule is bound to a protein, the longer correlation time of the complex means that the ^{31}P nuclei dipolar relaxation by nearby protons is significantly enhanced at low fields [7]. Under fast exchange conditions, the observed R_1 is then a weighted average of the very small R_1 of the unbound population and the much larger R_1 of the bound population. The effectiveness of dipolar relaxation depends on the number and proximity of nearby protons to the ^{31}P nuclei as well as magnetic field

strength. In 'high resolution' field cycling, samples are excited at high field, shuttled to low field for relaxation, then returned to the high field for detection of the residual magnetization of each nucleus of interest [5, 6]. The shuttling preserves the chemical shift differences of phosphorylated molecules allowing spin-lattice relaxation rates to be measured over a wide range of magnetic fields (11.7 to 0.003 T). In this field range both dipolar and CSA mechanisms contribute to the ^{31}P R_1 and the dependence of each of these features on magnetic field can be accounted for by equation [1]. The separation of the dipolar R_1 from CSA and its analysis (first term of equation [1]) yields a correlation time (τ) and a relaxation rate extrapolated to zero field (R_0). The sixth root of τ/R_0 is related to the averaged distance between the ^{31}P nuclei and the protons that relax it (Equation [2]). A key point in this experiment is that GMPR-bound and free ligands must be in fast exchange to detect the protein-induced relaxation behavior is that for each ^{31}P resonance, τ and R_0 characterize substrate and cofactor binding in the Michaelis complex.

Exchangeable protons contribute to relaxation of the substrate monophosphate in the hydride transfer complex.

Significant dipolar relaxation is most likely to arise from interactions between the ^{31}P nuclei and nonexchangeable protons attached to carbon atoms, either on the substrate/cofactor or the enzyme. Protons attached to heteroatoms can also contribute to ^{31}P relaxation, but these protons must be in slow exchange with solvent. Similarly, solvent protons may also contribute to relaxation if they are in slow exchange with bulk solvent. Inspection of the x-ray crystal structures identified both exchangeable and nonexchangeable protons in close proximity to the ^{31}P nuclei of both substrate and cofactors (Figure 2). Therefore, we carried out the field cycling experiments in D_2O instead of H_2O to assess the contribution of exchangeable protons and further assess the relevance of the substrate/cofactor conformations observed in the crystal structures to the conformations in the catalytically competent complexes in solution (Figure 3 and Table 1). At least three independent field cycling experiments were performed for each complex; the individual R_1 values were determined at a minimum of 15 different magnetic fields. If exchangeable protons make a significant contribution to ^{31}P relaxation, then R_0 should decrease (if τ is not significantly affected), and the ratio of of τ/R_0 should increase, implying an increase in r_{eff}.

For IMP in the E-IMP•$NADP^+$ complex in D_2O, the value of R_0 decreased roughly 3-fold. resulting in an approximately 3-fold increase of τ/R_0. Thus, exchangeable protons contribute to the relaxation of the ^{31}P of IMP in the hydride transfer complex. Our previous work indicated that the averaged ^{31}P-^{1}H distance (assuming $N_H = 1$) was 2.9 ± 0.2 Å for the ^{31}P of IMP in its $NADP^+$ complex [4]. Inspection of the IN structure identified three nonexchangeable protons and four exchangeable protons within 3 Å of the substrate ^{31}P (Figure 2A), so the D_2O effect is consistent with the IMP binding mode observed in the IN structure.

The substrate occupies the same binding site in the OUT crystal structure, again with six protons within 3 Å of the substrate ^{31}P, including the same three nonexchangeable protons, and the same backbone amides as in the IN structure (Figure 2B). If the deamination complex adopts the OUT structure, then the relaxation of the ^{31}P of GMP should also be

perturbed by D_2O. However, the value of τ/R_0 for the GMP ^{31}P in the cofactor complex is fairly large in H_2O, making an accurate measurement of the D_2O effect difficult. The errors in determining τ/R_0 in D_2O are large but similar to what is observed in H_2O (Table 1). Nonetheless, a three-fold increase in τ/R_0, as observed for IMP in the complex, is certainly not observed. Thus, predominantly nonexchangeable protons dominate the relaxation of the GMP ^{31}P in the ternary complex. The absence of a strong D_2O effect provides further evidence that the monophosphates of the two substrates must have different binding modes in their respective cofactor complexes. Intriguingly, in molecular simulations of the deamination reaction, the substrate monophosphate is displaced from its position in the crystal structure, such that only one nonexchangeable proton, a 5'-H, is within 3 Å of the ^{31}P nuclei of GMP (W. Yang, personal communication). This binding mode is more consistent with the observed relaxation.

The D_2O effect on ^{31}P relaxation provides evidence for different cofactor conformations in different steps of the catalytic cycle.

Previous field cycling experiments found that the dynamic processes associated with cofactor binding are different in the IMP and GMP complexes [4]. The cofactor is relatively constrained in the IMP complex, and more dynamic in the GMP complex. However, the values of τ/R_0 for the cofactor ^{31}P nuclei were similar in both complexes, so these experiments were unable to corroborate the distinct cofactor conformations expected for each partial reaction and observed in the crystal structures.

We evaluated the effect of D_2O on relaxation of the cofactor ^{31}P in the hope of gaining some insight into whether the cofactor binding modes resemble the conformations observed in the IN or OUT crystal structures. The presence of D_2O perturbed the relaxation of all three cofactor ^{31}P nuclei in the IMP complex (the values of τ/R_0 increased by approximately a factor of ~2 for all; Table 1), but had a smaller effect on the ^{31}P nuclei in the GMP complex. This observation suggests that more exchangeable protons contribute to the relaxation of the cofactor in complex with IMP. Inspection of the environments of the cofactor monophosphate in the IN and OUT structures revealed that the constellation of potential proton relaxers is very similar in both (Figure 2C,D), so the origin of the D_2O effect on this nuclei is not readily apparent. A clear difference is found in the potential proton relaxers in the vicinity of the cofactor diphosphates (Figure 2E,F). While similar numbers of nonexchangeable protons are observed within 4 Å of these nuclei in both the IN and OUT structures (15 and 14, respectively), more exchangeable protons are observed in the IN structure (13) versus the OUT (8). Therefore, we tentatively conclude that the cofactor conformation in the IMP complex resembles the IN structure, and the conformation in the GMP complex resembles the OUT conformation, as originally proposed.

Deoxynucleotides are poor substrates for GMPR.

The crystal structures reveal that the 2'-OH and 3'-OH of both IMP and GMP form hydrogen bonds with Asp219 (Figure 1B; [13,14]). We assayed the reactions of GMPR with dIMP and dGMP to probe the importance of these interactions for catalysis. As expected, dIMP and dGMP are poor substrates for GMPR (Table 2). The values of K_m increased by factors of 5–6 relative to the ribose substrates, while the values of K_m for the cofactors

increased by approximately a factor of 1.6–2. The value of k_{cat} decreased by a factor of 15 relative to GMP and the value of V_{max}/[E] for the reverse reaction decreased by a factor of 9 relative to IMP (at fixed [NH_4^+] = 20 mM; it is not possible to saturate the reaction with respect to NH_4^+). The rate constant of the partial hydride transfer reaction between dIMP and $NADP^+$ is lower by a factor of 7.5 relative to that of IMP (Table 2 and Supporting Figures S1 and S2). The equilibrium constants for the partial reactions estimated from the [NADPH]/[E] are ~0.2 for IMP and ~0.08 for dIMP. The individual rate constants can also be estimated: for IMP, k_f = ~0.07 s^{-1} and k_r = ~0.4 s^{-1} while for dIMP, k_f = ~0.006 and k_r = ~0.06 for dIMP. Note that the values of k_r for IMP and dIMP are comparable to the values of k_{cat} for the reactions of GMP and dGMP, respectively. These observations indicate that hydride transfer is rate-limiting for both ribose and deoxyribose substrates. Note also that these rate constants are slow relative to the time-scale needed for fast exchange on the NMR time scale. This indicates that the E-XMP*•NADPH complex should not contribute to the ^{31}P relaxation.

The dynamics of the cofactor complexes of dGMP/dIMP are disregulated relative to GMP/IMP.

The ^{31}P relaxation experiments revealed that the dynamic properties of the cofactor complexes with dGMP and dIMP are dramatically different from their ribose counterparts (Figure 4 and Table 3). In the E•GMP•$NADP^+$ complex, GMP is constrained and the cofactor is dynamic as reflected in the values of τ extracted with a simple single dipolar component fit [4]. However, when dGMP was the substrate, the substrate is dynamic and the cofactor is constrained. The value of τ decreased to 36 ns for the ^{31}P of dGMP, similar to that observed for the substrate in the hydride transfer complex. The value of τ/R_0 also decreased, indicating that the monophosphate of dGMP is closer to proton relaxers, also as observed for the substrate in the hydride transfer complex. For the cofactor ^{31}P nuclei, the values of τ increased to 70–110 ns, similar to the cofactor in the hydride transfer complex. Note that the values of τ/R_0 do not distinguish the conformations of the cofactor in the hydride transfer and deamination complexes, and similar values are observed for the cofactor ^{31}P nuclei in E•dGMP•$NADP^+$, so no conclusions can be made about the cofactor binding mode. Taken together, the dGMP-cofactor complex is primed for hydride transfer, not deamination.

Similarly, the dynamic characteristics of the dIMP-cofactor complex were very different than those observed with E•IMP•$NADP^+$. Whereas IMP is more dynamic than the cofactor, both ligands are relatively constrained in the dIMP complex. The environment of the substrate monophosphate is also different in this complex, with $\tau/R_0 = 13 \times 10^{-8}$ s^2 for dIMP versus 3.3×10^{-8} s^2 for IMP. This value indicates that the dIMP substrate ^{31}P nucleus is farther away from proton relaxers, and suggests a conformation/environment similar to in the deamination complex. Larger values of τ/R_0 are also observed for the cofactor ^{31}P nuclei, which suggests the presence of an altered cofactor binding mode. Thus, neither the conformation nor the dynamics of the dIMP-cofactor complex appear conducive to hydride transfer.

Asp219 coordinates the dynamics of enzyme bound substrates and cofactors.

Asp219 makes hydrogen bonds with both the 2'-OH and 3'-OH of the ribose substrates, and therefore might be expected to be critical for holding the substrate in position for catalysis (Figure 1B) [13]. The profound changes in dynamics observed with dGMP and dIMP prompted us to investigate the effects of substituting Asp219 with Ala. Not surprisingly, the mutation of Asp219 to Ala severely diminished enzyme activity. The values of K_m for GMP and NADPH increased by factors of 120 and 12, respectively, while the value of k_{cat} decreased by a factor of 27 (Table 3). Comparable changes where observed in the reaction of IMP (K_m increased 48-fold), $NADP^+$ (K_m increased 8-fold) and NH_4^+ (V_{max}/[E] decreased by a factor of 45). D219A also catalyzed the reaction between IMP and $NADP^+$ in the absence of NH_4^+. However, unlike the reaction of the wild-type enzyme, which reached equilibrium within 10 sec (Supporting Figure 1), the progress curve for the D219A reaction displayed a burst of NADPH production followed by a slower phase that could be fit to a steady state rate (Supporting Figure S3). This second phase is faster than the rate of NADPH production observed in longer progress curves (Supporting Figure S3), suggesting that hydride transfer is not rate-limiting for the reaction of D219A. We suggest that the slow production of NADPH may be the result of slow dissociation of NADPH and off-pathway hydrolysis of E-XMP*. Importantly, the rate of the reaction under the conditions of the field cycling experiments is approximately 40% of that observed under saturating substrate conditions, indicating that the fraction of bound enzyme is 0.4 (Supporting Figure 3).

^{31}P field cycling experiments revealed that the values of τ are similar (108–143 ns) for all of the substrate and cofactor ^{31}P nuclei in both D219A ternary complexes, as would be expected if τ was dominated by rotational relaxation of the enzyme complex (Figure 5 and Table 3; note that the value of τ does not depend on the fraction of substrate bound enzyme – only R_0 is affected). This observation suggests that both substrates and cofactor are constrained within the ternary complexes in the absence of Asp219. Unlike the wild-type enzyme, no difference is observed in the relaxation of GMP and IMP in their respective cofactor complexes with D219A (Figure 5). The values of τ/R_0 for the substrate monophosphates are similar to that observed for IMP in the ternary complex of wild-type enzyme (Table 3; note that the correction of the bound enzyme in the IMP complex has no effect on this conclusion). These observations suggest that GMP can no longer access the distinct binding mode associated with the deamination reaction in D219A and the IMP binding site no longer has the dynamic mode associated with the hydride transfer reaction.

While the cofactor was clearly constrained in both substrate complexes with D219A, the effects of this mutation on the cofactor binding modes are difficult to assess. The mutation increases values of τ/R_0 for the cofactor ^{31}P nuclei in the GMP complex, perhaps suggesting the presence of a new binding mode. However, the errors for these values overlap with those observed in the wild-type complex. The need to correct for the fraction of bound enzyme further obscures the effects of the mutation on the cofactor conformation in complex with IMP. Therefore, it is possible that D219 also controls cofactor conformation in addition to cofactor dynamics. Interestingly, additional cofactor binding modes are uncovered in molecular simulations (W. Yang, personal communication), so the broad range in τ/R_0

values observed in the field cycling experiment may reflect extensive conformational heterogeneity that is not captured in the x-ray crystal structures.

CONCLUSIONS

Our experiments reveal multiple binding modes for substrates and $NADP^+$ in catalytically competent complexes of GMPR. Figure 6 summarizes these findings. Different binding modes are observed for substrates GMP and IMP. This observation contrasts with currently available crystal structures of inactive complexes that observe a single binding mode for both substrates. Moreover, distinct dynamic states are associated with each step in the catalytic cycle. The substrate is constrained and the cofactor is dynamic in the Michaelis complex for the deamination reaction, while the substrate is dynamic and the cofactor is constrained in the Michaelis complex for hydride transfer. A comparatively small structural perturbation, the substitution of H for OH, perturbs these binding modes and dynamic states, with a detrimental effect on catalysis. Lastly, Asp219, rather than simply holding substrates in position for catalysis, plays a critical role in modulating the dynamics of both substrates and cofactor. Thus, these findings provide new insights into how distal portions of the substrate promote catalysis.

Supplementary Material

Refer to Web version on PubMed Central for supplementary material.

Acknowledgements:

This work was supported by the National Institutes of Health (GM054403 to LH). Molecular graphics images were produced using the UCSF Chimera package from the Computer Graphics Laboratory, University of California, San Francisco (supported by NIGMS P41-GM103311). We thank Gregory Patton for the D219A expression plasmid.

REFERENCES

[1]. Schwans JP, Kraut DA, and Herschlag D (2009) Determining the catalytic role of remote substrate binding interactions in ketosteroid isomerase, Proc Natl Acad Sci U S A 106, 14271–14275. [PubMed: 19706511]

[2]. Richard JP, Amyes TL, Goryanova B, and Zhai X (2014) Enzyme architecture: on the importance of being in a protein cage, Curr Opin Chem Biol 21, 1–10. [PubMed: 24699188]

[3]. Leatherbarrow RJ, and Fersht AR (1987) Investigation of transition-state stabilization by residues histidine-45 and threonine-40 in the tyrosyl-tRNA synthetase, Biochemistry 26, 8524–8528. [PubMed: 3126804]

[4]. Rosenberg MM, Redfield AG, Roberts MF, and Hedstrom L (2016) Substrate and Cofactor Dynamics on Guanosine Monophosphate Reductase Probed by High Resolution Field Cycling 31P NMR Relaxometry, J Biol Chem 291, 22988–22998. [PubMed: 27613871]

[5]. Redfield AG (2012) High-resolution NMR field-cycling device for full-range relaxation and structural studies of biopolymers on a shared commercial instrument, Journal of biomolecular NMR 52, 159–177. [PubMed: 22200887]

[6]. Roberts MF, and Redfield AG (2004) High-resolution 31p field cycling NMR as a probe of phospholipid dynamics, J Am Chem Soc 126, 13765–13777. [PubMed: 15493936]

[7]. Pu M, Feng J, Redfield AG, and Roberts MF (2009) Enzymology with a spin-labeled phospholipase C: soluble substrate binding by 31P NMR from 0.005 to 11.7 T, Biochemistry 48, 8282–8284. [PubMed: 19663462]

[8]. Pu M, Orr A, Redfield AG, and Roberts MF (2010) Defining specific lipid binding sites for a peripheral membrane protein in situ using subtesla field-cycling NMR, J Biol Chem 285, 26916–26922. [PubMed: 20576615]

[9]. Gradziel CS, Wang Y, Stec B, Redfield AG, and Roberts MF (2014) Cytotoxic amphiphiles and phosphoinositides bind to two discrete sites on the Akt1 PH domain, Biochemistry 53, 462–472. [PubMed: 24383815]

[10]. Wei Y, Stec B, Redfield AG, Weerapana E, and Roberts MF (2015) Phospholipid-binding sites of phosphatase and tensin homolog (PTEN): exploring the mechanism of phosphatidylinositol 4,5-bisphosphate activation, J Biol Chem 290, 1592–1606. [PubMed: 25429968]

[11]. Wilmanns M, Hyde CC, Davies DR, Kirschner K, and Jansonius JN (1991) Structural conservation in parallel beta/alpha-barrel enzymes that catalyze three sequential reactions in the pathway of tryptophan biosynthesis, Biochemistry 30, 9161–9169. [PubMed: 1892826]

[12]. Nagano N, Orengo CA, and Thornton JM (2002) One fold with many functions: the evolutionary relationships between TIM barrel families based on their sequences, structures and functions, J Mol Biol 321, 741–765. [PubMed: 12206759]

[13]. Patton GC, Stenmark P, Gollapalli DR, Sevastik R, Kursula P, Flodin S, Schuler H, Swales CT, Eklund H, Himo F, Nordlund P, and Hedstrom L (2011) Cofactor mobility determines reaction outcome in the IMPDH and GMPR (beta-alpha)8 barrel enzymes, Nat Chem Biol 7, 950–958. [PubMed: 22037469]

[14]. Li J, Wei Z, Zheng M, Gu X, Deng Y, Qiu R, Chen F, Ji C, Gong W, Xie Y, and Mao Y (2006) Crystal structure of human guanosine monophosphate reductase 2 (GMPR2) in complex with GMP, J Mol Biol 355, 980–988. [PubMed: 16359702]

[15]. Gasteiger E, Hoogland C, Gattiker A, Duvaud S, Wilkins MR, Appel RD, and A., B. (2005) The Proteomics Protocols Handbook, Humana Press, New York.

[16]. Roberts MF, Cui Q, Turner CJ, Case DA, and Redfield AG (2004) High-resolution field-cycling NMR studies of a DNA octamer as a probe of phosphodiester dynamics and comparison with computer simulation, Biochemistry 43, 3637–3650. [PubMed: 15035634]

[17]. Pettersen EF, Goddard TD, Huang CC, Couch GS, Greenblatt DM, Meng EC, and Ferrin TE (2004) UCSF Chimera- a visualization system for exploratory research and analysis, J. Comp. Chem. 25, 1605–1612. [PubMed: 15264254]

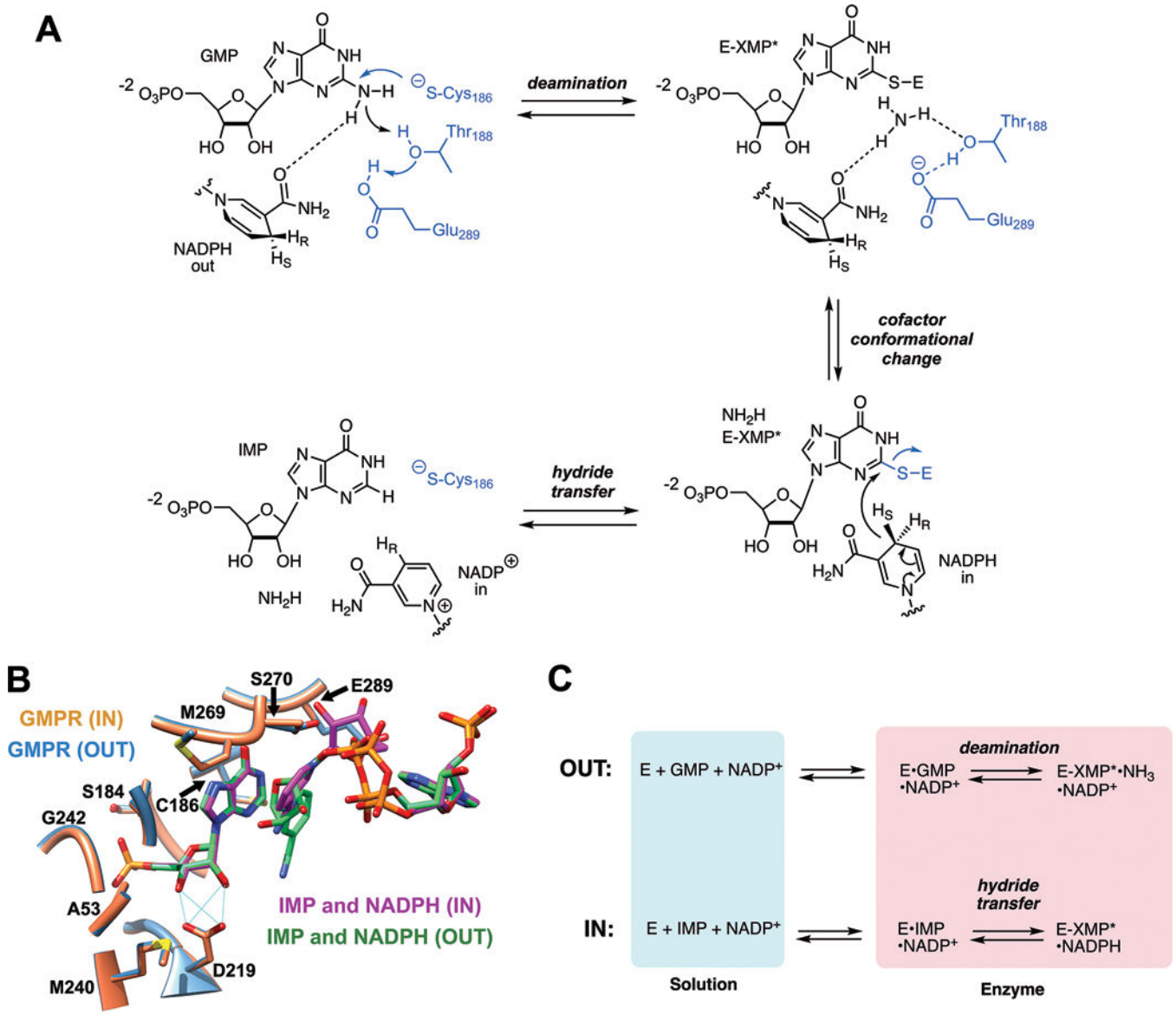

Figure 1. The reactions and structure of GMPR.

(*A*) The GMPR reaction. (*B*) GMPR active sites with NADPH in the IN and OUT conformations are displayed (PDB entry 2C6Q). Residues in contact with IMP are shown. This figure was produced with UCSF Chimera [17]. (*C*) The partial reactions catalyzed by GMPR.

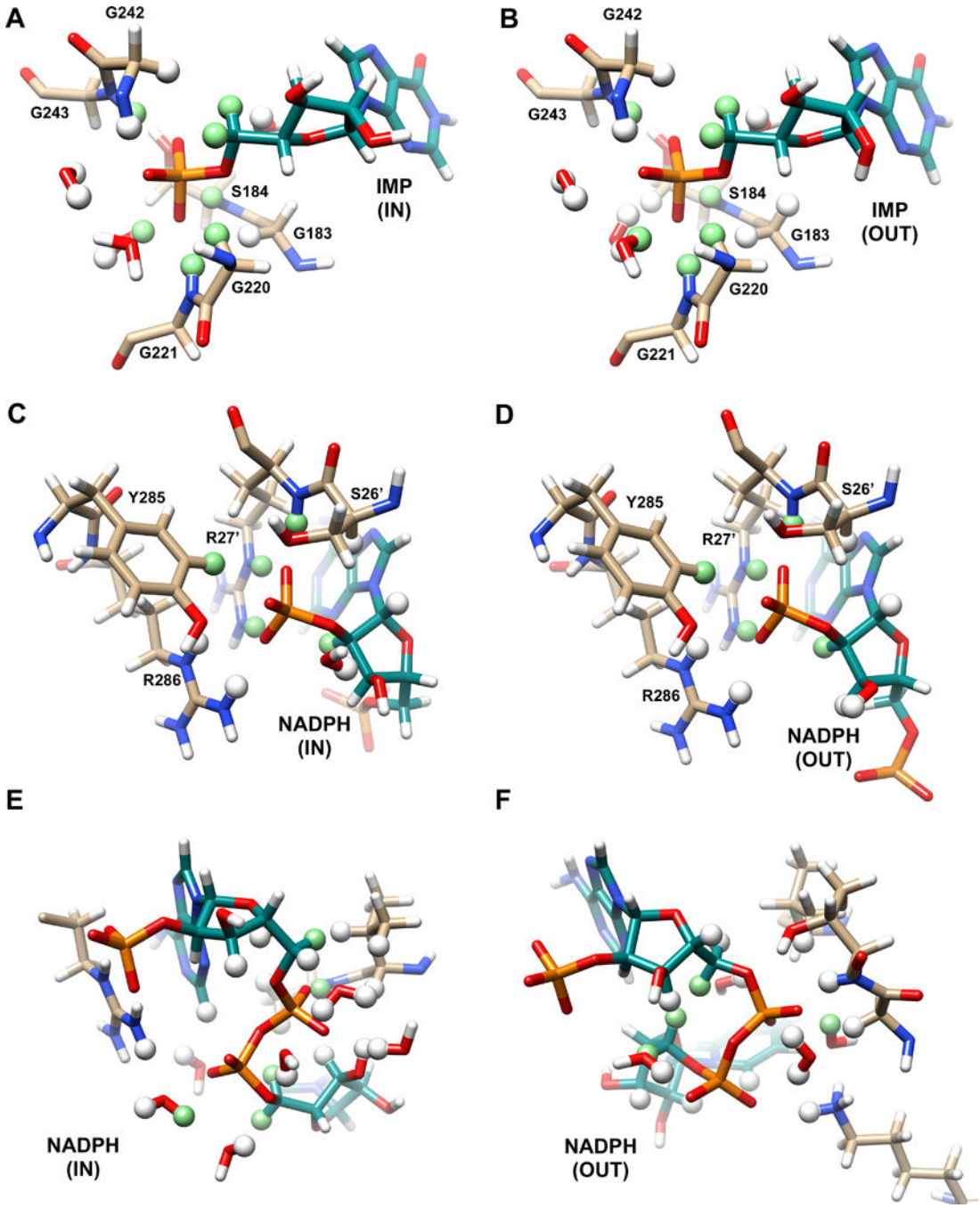

Figure 2. Candidate proton relaxers.

Hydrogen atoms within 4 Å of the phosphorus atom of IMP (*A,B*), of the NADPH monophosphate P (*C,D*) and the NADPH diphosphates P atoms (E,F) in the IN (*A,C,E*) and OUT (*B,D,F*) complexes (PDB entry 2C6Q). Protons within 4 Å of the phosphorus are shown as a ball, protons within 3 Å are colored light green. This figure was produced with UCSF Chimera [17].

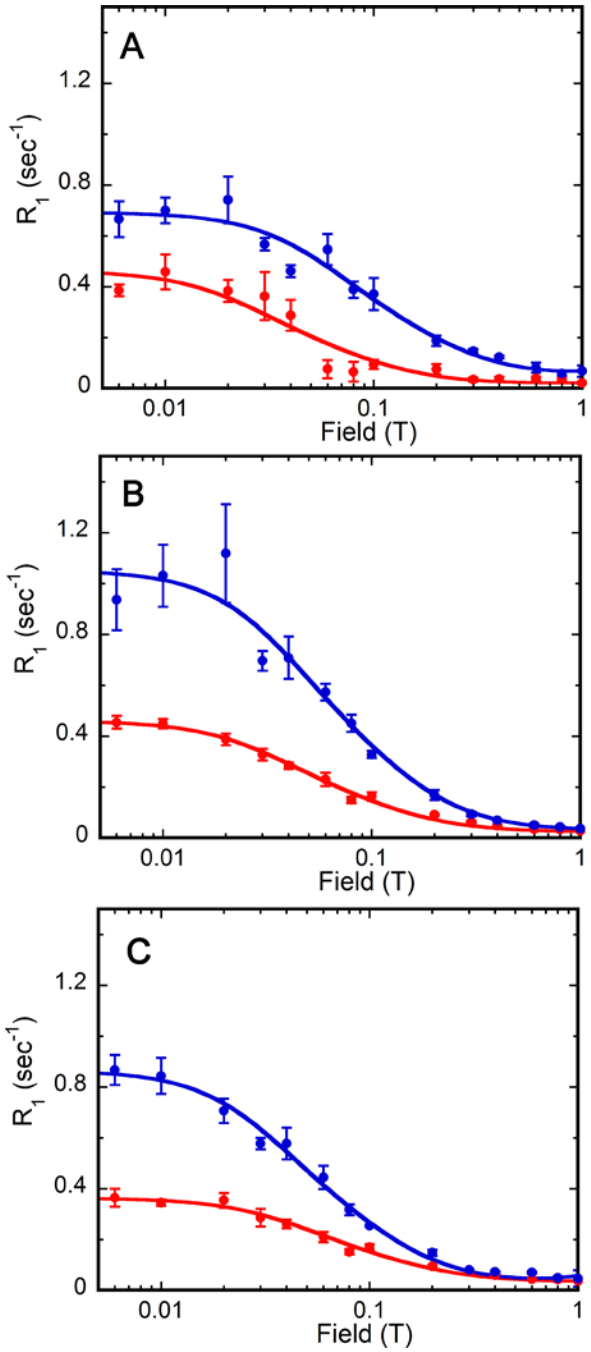

Figure 3. Magnetic field dependence of substrate and cofactor ^{31}P R_1 in E•GMP•NADP$^+$ and E•IMP•NADP$^+$ complexes in D_2O.

Samples (E•GMP•NADP$^+$ in *red* and E•IMP•NADP$^+$ in *blue*) are in 75 mM Tris-HCl, pH 7.8, 100 mM KCl, 1 mM DTT and 0.5 mM EDTA: (*A*) substrate monophosphate, (*B*) cofactor monophosphate, and (*C*) cofactor diphosphates. The error bars are the standard error in R_1 from the exponential fit of signal magnitude versus delay time. The data shown are for one of the three independent experiments.

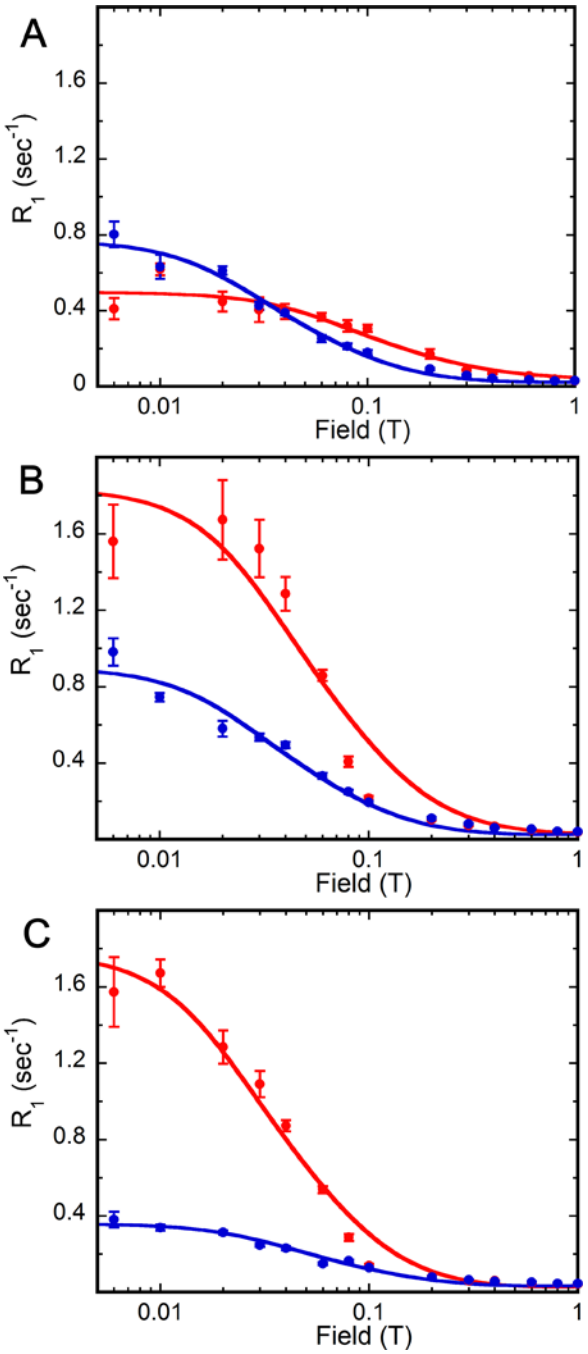

Figure 4. Magnetic field dependence of deoxy substrate and cofactor ^{31}P R_1 in E•dGMP•NADP$^+$ and E•dIMP•NADP$^+$ complexes.

Samples (E•dGMP•NADP$^+$ in *red* and E•dIMP•NADP$^+$ in *blue*) are in 75 mM Tris-HCl, pH 7.8, 100 mM KCl, 1 mM DTT and 0.5 mM EDTA. Data for (*A*) deoxy substrate monophosphate, (*B*) cofactor monophosphate and (*C*) cofactor diphosphates are shown. Error bars are as described in Figure 3.

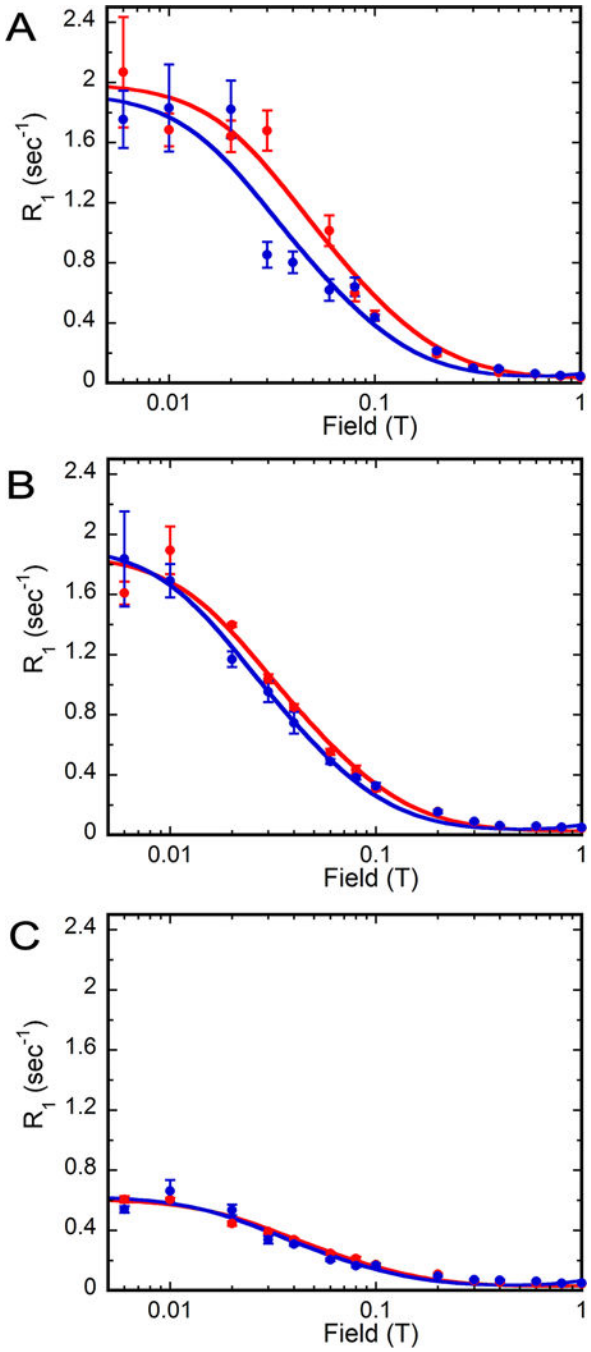

Figure 5. Magnetic field dependence of substrate and cofactor ^{31}P R_1 in D219A•GMP•NADP$^+$ and D219A•IMP•NADP$^+$ complexes.

Samples (D219A•GMP•NADP$^+$ in *red* and D219A•IMP•NADP$^+$ in *blue*) are in 75 mM Tris-HCl, pH 7.8, 100 mM KCl, 1 mM DTT and 0.5 mM EDTA: (*A*) substrate monophosphate, (*B*) cofactor monophosphate, and (*C*) cofactor diphosphates. Error bars are described in Figure 3.

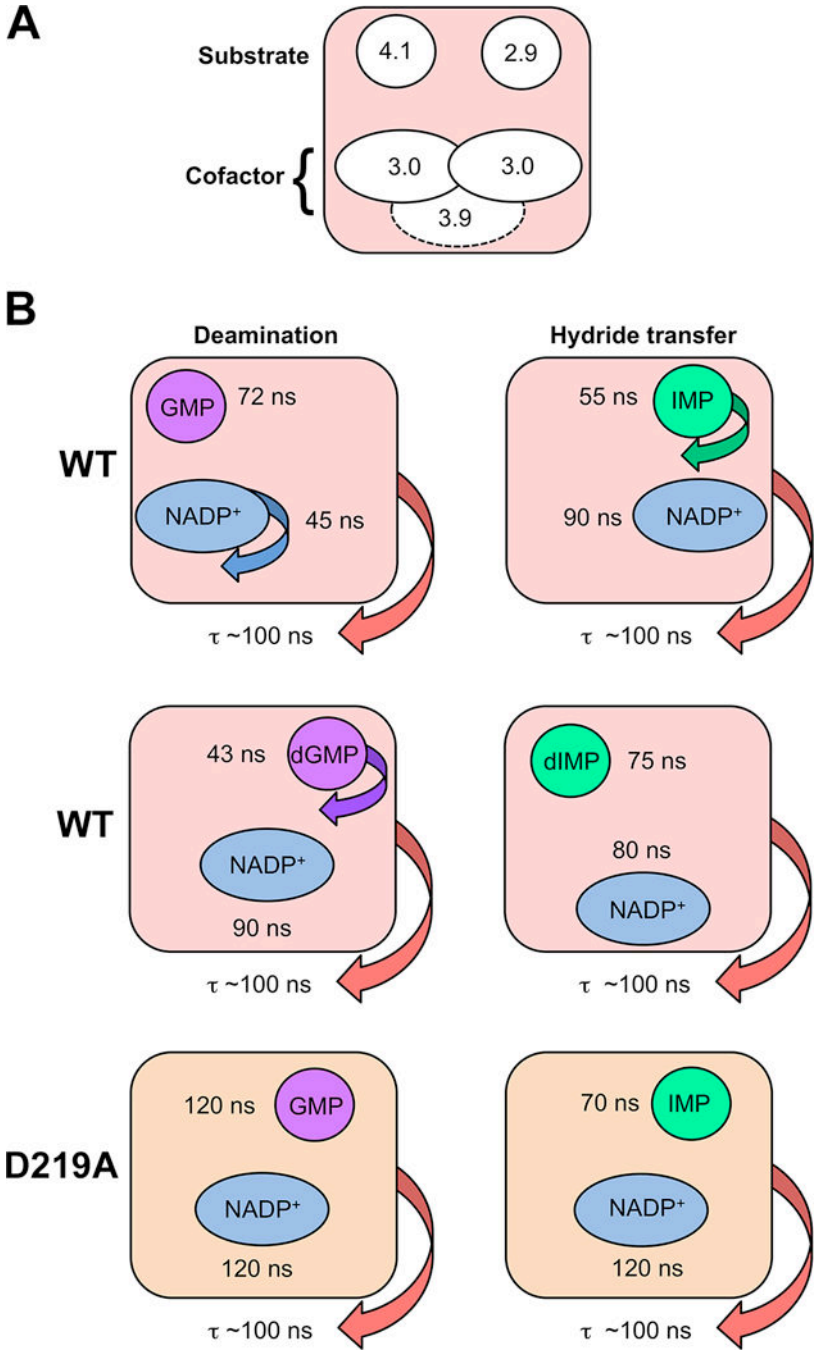

Figure 6. Dynamic characteristics of GMPR complexes revealed by high resolution ^{31}P field cycling NMR relaxometry.

(*A*) Multiple binding modes for substrate and cofactors. Two distinct binding modes are observed for IMP and GMP in their catalytically active $NADP^+$ complexes. The cofactor also has two distinct binding modes in these complexes as shown by the effects of D_2O on relaxation, albeit with similar ^{31}P-proton relaxer distances. These binding modes are indicated by the positions of the two ellipses. When the binding mode cannot be distinguished by the values of τ/R_0, the ellipse is positioned in the center. A third conformation, indicated by the dashed ellipse, is observed in the dIMP-cofactor complex.

The extrapolated ^{31}P-proton relaxer distances are show in Å. (*B*) Distinct dynamic states are observed in wild-type enzyme and D219A and with ribose and deoxyribose substrates as evidenced by values of τ.

Table 1.

Effect of D_2O on ^{31}P dipolar relaxation parameters for substrate and cofactor in GMPR ternary complexes extracted from field cycling relaxometry.

Values for τ, R_0 and τ/R_0 are the average and standard deviation from 3 independent experiments.

^{31}P	Complex	Solvent	τ (ns)	R_0 (s^{-1})	$\tau/R_0 \times 10^8$ (s^2)
IMP	WT•IMP •$NADP^+$	H_2O [a]	55 ± 12	1.9 ± 0.9	3.3 ± 1.1
		D_2O	45 ± 1	0.6 ± 0.2	8 ± 3
GMP	WT•GMP •$NADP^+$	H_2O [a]	72 ± 13	0.30 ± 0.02	24 ± 5
		D_2O	77 ± 16	0.3 ± 0.1	24 ± 12
$NADP^+$ mono-phosphate	WT•IMP •$NADP^+$	H_2O [a]	103 ± 23	2.9 ± 1.2	3.8 ± 0.9
		D_2O	62 ± 3	0.7 ± 0.3	9 ± 4
	WT•GMP •$NADP^+$	H_2O [a]	47 ± 11	0.6 ± 0.1	8.6 ± 2.3
		D_2O	55 ± 18	0.4 ± 0.1	13 ± 5
$NADP^+$ diphosphates	WT•IMP •$NADP^+$	H_2O [a]	88 ± 13	1.4 ± 0.3	6.6 ± 1.2
			82 ± 17	1.6 ± 0.3	5.1 ± 0.9
		D_2O	70 ± 5	0.6 ± 0.3	12 ± 7
			58 ± 8	0.6 ± 0.3	10 ± 5
	WT•GMP •$NADP^+$	H_2O [a]	44 ± 5	0.5 ± 0.2	9.2 ± 2.4
			45 ± 8	0.5 ± 0.1	9.3 ± 2.5
		D_2O	50 ± 9	0.3 ± 0.1	15 ± 5
			50 ± 1	0.3 ± 0.1	15 ± 3

[a] Values from 4.

Table 2.
Kinetic parameters for WT and D219A GMPR.

Reactions were performed in 75 mM Tris, pH 7.8, 100 mM KCl, 1 mM DTT and 0.5 mM EDTA at 25 °C. NADPH consumption/formation was monitored as described in Methods. Values are the average and standard error of at least two independent experiments. "K_m(S)" denotes the K_m of GMP, dGMP, IMP or dIMP, as appropriate. "k" denotes k_{cat} for the reaction of dGMP+NADPH, V_m/[E] for the reaction of dIMP+$NADP^+$ +NH_3 and k_{obs} for the partial reaction of dIMP+$NADP^+$.

Enzyme	Reaction	K_m (S) (μM)	K_m (cofactor) (μM)	k (s^{-1})
WT	GMP + NADPH [a]	3.2 ± 0.5	10.1 ± 0.8	0.35 ± 0.01
	dGMP + NADPH [b]	15 ± 3	16 ± 4	0.023 ± 0.002
D219A	GMP + NADPH [c]	380 ± 130	120 ± 20	0.013 ± 0.003
WT	IMP + $NADP^+$ + NH_3 [d]	23 ± 6	50 ± 16	0.018 ± 0.009
	dIMP + $NADP^+$ + NH_3 [e]	140 ± 20	109 ± 28	0.002 ± 0.001
D219A	IMP + $NADP^+$ + NH_3 [f]	1100 ± 240	420 ± 220	(4.0 ± 0.3) x 10^{-4}
WT	IMP + $NADP^+$ [g]	n.a.	n.a.	0.49 ± 0.01 (16%)
	dIMP + $NADP^+$ [g]	n.a.	n.a.	0.064 ± 0.001 (10%)
D219A	IMP + $NADP^+$ [g]	n.a.	n.a.	0.055 ± 0.003 (2.8%)

[a] Values from 13.

[b] Reactions performed at saturating concentrations of the fixed substrate dGMP (200 μM) and NADPH (150 μM).

[c] Reactions performed at saturating concentrations of GMP (2 mM) and NADPH (600 μM).

[d] Reactions performed at saturating concentrations of IMP (500 μM), $NADP^+$ (500 μM) and NH_4^+ (20 mM).

[e] Reactions performed at saturating concentrations of the fixed substrate, IMP (1 mM) and $NADP^+$ (500 μM).

[f] Reactions performed at saturating concentrations of the fixed substrate, IMP (10 mM) and $NADP^+$ (3 mM).

[g] Reactions performed at saturating conditions as described above. The percentage of NADPH produced per active site at equilibrium is shown in parentheses; n.a., not applicable

Table 3.

^{31}P dipolar relaxation parameters (from field cycling) for NADP$^+$ complexes of GMPR or mutant D219A with GMP, IMP or deoxy-substrates (dGMP and dIMP).

^{31}P	Complex	N [a]	τ (ns)	R_0 (s^{-1})	τ /R_0 × 10^8(s^2)
(d)IMP	WT•dIMP •NADP$^+$	3	75 ± 30	0.8 ± 0.3	10 ± 5
	D219A•IMP •NADP$^+$	2	70 ± 26	1.7 ± 0.3 (4.3 ± 0.7) [c]	4.1 ± 1.7 (1.6 ± 0.7) [c]
(d)GMP	WT•dGMP •NADP$^+$	3	43 ± 12	0.4 ± 0.2	11 ± 6
	D219A•GMP •NADP$^+$	4	120 ± 34	3.8 ± 1.2	3.1 ± 1.3
NADP$^+$ mono-phosphate	WT•dIMP •NADP$^+$	3	92 ± 18	0.8 ± 0.2	11 ± 3
	D219A•IMP •NADP$^+$	2	139 ± 9	1.95 ± 0.02 (4.88 ± 0.05) [c]	7.1 ± 0.5 (2.8 ± 0.2) [c]
	WT•dGMP •NADP$^+$ [b]	3	75 ± 8	1.5 ± 0.5	5 ± 2
	D219A•GMP •NADP$^+$ [d]	4	125 ± 8	2.3 ± 0.3	5.3 ± 0.8
NADP$^+$ diphosphates	WT•dIMP •NADP$^+$	3	61 ± 23	0.3 ± 0.1	18 ± 8
			85 ± 21	0.4 ± 0.1	23 ± 6
	D219A•IMP •NADP$^+$	2	113 ± 6	0.60 ± 0.02 (1.50 ± 0.05) [c]	18 ± 1 (7.2 ± 0.4) [c]
			112 ± 4	0.60 ± 0.04 (1.5 ± 0.1) [c]	18 ± 2 (7.2 ± 0.8) [c]
	WT•dGMP •NADP$^+$	3	101 ± 27	1.6 ± 0.5	6.3 ± 3
			98 ± 23	1.6 ± 0.4	6.2 ± 3
	D219A•GMP •NADP$^+$ [d]	4	137 ± 32	0.86 ± 0.15	16 ± 5
			114 ± 13	0.8 ± 0.1	15 ± 3

[a] N is the number of independent experiments averaged to obtain the values tabulated.

[c] R_0 corrected for the fraction of E•IMP•NADP$^+$ compared to total enzyme (0.40).